Journal of Solid State Chemistry **160,** 474–481 (2001)
doi:10.1006/jssc.2001.9323, available online at http://www.idealibrary.com on IDEAL®

RAPID COMMUNICATION

Transport Properties of $Bi_{2-x}In_xSe_3$ Single Crystals

J. Navrátil,* T. Plecháček,* J. Horák,* S. Karamazov,† P. Lošťák,† J. S. Dyck,‡ W. Chen,‡ and C. Uher‡

*Joint Laboratory of Solid State Chemistry of the Academy of Sciences of the Czech Republic and the University of Pardubice, Studentská 84, 532 10 Pardubice, Czech Republic; †Faculty of Chemical Technology, University of Pardubice, Čs. legií Square 565, 532 10 Pardubice, Czech Republic; and ‡Department of Physics, University of Michigan, Ann Arbor, MI 48109, USA

Received February 5, 2001; in revised form April 4, 2001; accepted May 14, 2001

The paper reports on the temperature dependence of the electrical and thermal conductivity, Hall constant, and Seebeck coefficient of $Bi_{2-x}In_xSe_3$ ($x = 0$, 0.2, 0.4) single crystals measured over the temperature range from 2 to 300 K. One single-valley conduction band model is used to interpret relations among transport coefficients. The data analysis relies on the use of a mixed carrier scattering mechanism consisting of acoustic scattering and scattering on ionized impurities. The effect of In incorporation into the Bi_2Se_3 crystal lattice on the individual components of thermal conductivity is evaluated and discussed.

Key Words: **transport properties; reflectance; narrow-gap semiconductors; tetradymite structure; Bi_2Se_3; indium incorporation; carrier scattering.**

INTRODUCTION

Solid solutions on the basis of narrow-band layered semiconductors $A_2^{V}B_3^{VI}$ (where A = Bi, Sb and B = Se, Te) of tetradymite structure (space group $R\bar{3}m - D_{3d}^5$) find applications in the field of thermoelectric devices (1). Therefore materials of this type are an object of both theoretical and applied research.

The phase diagram (2, 3) suggests that both components of the pseudobinary Bi_2Se_3–In_2Se_3 system should form solid solutions of the form $Bi_{2-x}In_xSe_3$ with tetradymite structure. This has, indeed, been corroborated by transport measurements (4). Beyond these investigations, little is known of the properties of these solid solutions. Especially incomplete is the information concerning transport properties of single crystals.

In our earlier works, we described the method of growing single crystals and we characterized them by measuring their lattice parameters, some basic electrical properties (5), and reflectance and transmittance in the infrared region (6, 7). Although thermal conductivity of Bi_2Se_3 was measured (8), the temperature range was limited to 100–300 K. Heat transport in $Bi_{2-x}In_xSe_3$ crystals has not been studied yet.

In this paper we present and discuss the temperature dependence of the electrical and thermal conductivity, Hall constant, and Seebeck coefficient. We interpret the data assuming a single band model. Although hints of the existence of a second conduction band in Bi_2Se_3 have been reported, the data are incomplete (9, 10). Furthermore, no data are available at all regarding how the parameters describing such a second band vary in the presence of In. In our analysis we pay special attention to the influence of specific scattering mechanisms governing the transport process—acoustic and ionized impurity scattering. By taking into consideration the respective contributions of the two scattering mechanisms we are able to determine the electronic term of thermal conductivity. By subtracting the electronic term from the total thermal conductivity we determine the lattice thermal conductivity, and we analyze its temperature dependence.

EXPERIMENTAL

Preparation of Single Crystals

The starting polycrystalline $Bi_{2-x}In_xSe_3$ material was synthesized from elements of 5N purity in evacuated conical silica ampoules at 1073 K for 48 h. The growth of the single crystals was carried out in the same ampoules by a modified Bridgman method using a suitable temperature gradient and a pulling rate of 0.8 mm/h (5).

The obtained single crystals, typically 60 mm in length and 8 mm in diameter, could be easily cleaved. Their trigonal axis (c-axis) was always perpendicular to the pulling direction so that the (0001) crystal plane was parallel to the ampoule axis. The orientation of the cleavage faces was

0022-4596/01 $35.00

checked using the Laue back-reflection method, which confirmed that these faces were always (0001). The indium content in the crystals was determined by a Kevex Delta 5 energy dispersive X-ray analyzer with a Quantum detector.

Characterization of the Crystals

The single crystals were characterized by measurement of the thermal transport parameters (thermopower and thermal conductivity), Hall constant, electrical conductivity, and reflectance spectra in the plasma resonance frequency region. Because of extreme difficulty in cutting reasonably sized crystals with their long edges along the crystallographic c-axis, we have made measurements in the direction perpendicular to the c-axis.

Thermopower and thermal conductivity were determined using a longitudinal steady-state technique in a cryostat equipped with two radiation shields. Thermal gradients were measured with the aid of fine chromel-constantan differential thermocouples, and a miniature strain gauge served as a heater. In spite of trying to eliminate all sources of stray heat, it is not possible to entirely avoid losses of heat via radiation. This is a particularly important issue at elevated temperatures (above about 150 K) and in measuring samples of low thermal conductivity such as our single crystals. Depending on the aspect ratio of the sample, the radiation loss may artificially enhance the measured value of the thermal conductivity at 300 K by as much as 20%. In order to determine the radiation loss experimentally, we made a subsequent measurement with the sample detached from the heat sink (sample hangs by its thin connecting wires) and we determined the amount of heat needed by the heater that raises the temperature of the entire sample to the same average temperature as during the actual measurement of the thermal conductivity. The values of the thermal conductivity were then corrected for this radiation loss.

For Seebeck probes we used fine copper wires that had previously been calibrated, and their thermopower contribution was subtracted from the measured sample thermopower. The Hall effect and electrical conductivity were studied using a Linear Research ac bridge with 16-Hz excitation in a magnet cryostat capable of fields up to 5 T. Measurements of these parameters were made over the temperature range 2–300 K. The use of the ac technique in measuring the galvanomagnetic properties eliminates the contribution of the Peltier effect, which would otherwise be superimposed on the purely ohmic response.

Spectral dependencies of the reflectance in the plasma resonance frequency region were measured at room temperature in unpolarized light on natural (0001) cleavage faces using a Biorad FTS 45 FT-IR spectrometer. The geometry of the experiment was such that the electric field vector E of the electromagnetic radiation was always perpendicular to the c-axis, i.e., $E \perp c$.

RESULTS AND DISCUSSION

Temperature dependencies of the Hall constant $R_H(B \| c)$, electrical conductivity $\sigma_\perp$ (perpendicular to the c-axis), thermal conductivity $\kappa_\perp$ (perpendicular to the c-axis), and Seebeck coefficient $S(\Delta T \perp c)$ of an undoped Bi_2Se_3 and two crystals with a high concentration of incorporated In atoms are given in Figs. 1–4. It is evident that the increasing content of incorporated In atoms results in a decrease of the electrical and thermal conductivity, an increase of the Hall constant and changes in the behavior of the Seebeck coefficient. The inset to Fig. 3 shows the Hall moblility, $\mu_H = R_H\sigma_\perp$. One can see that μ_H decreases as the In concentration is increased. The weak temperature dependence suggests a mixed scattering mechanism including both acoustic phonons (near room temperature) and impurities. We first describe the data on pure Bi_2Se_3.

Undoped Bi_2Se_3 Single Crystal

With the aim of explaining relations between the various transport coefficients measured on the pure Bi_2Se_3, the free carrier density and the Fermi level have been calculated making the following assumptions:

(a) the conduction band of Bi_2Se_3 can be described in terms of a single-valley one-conduction-band model,

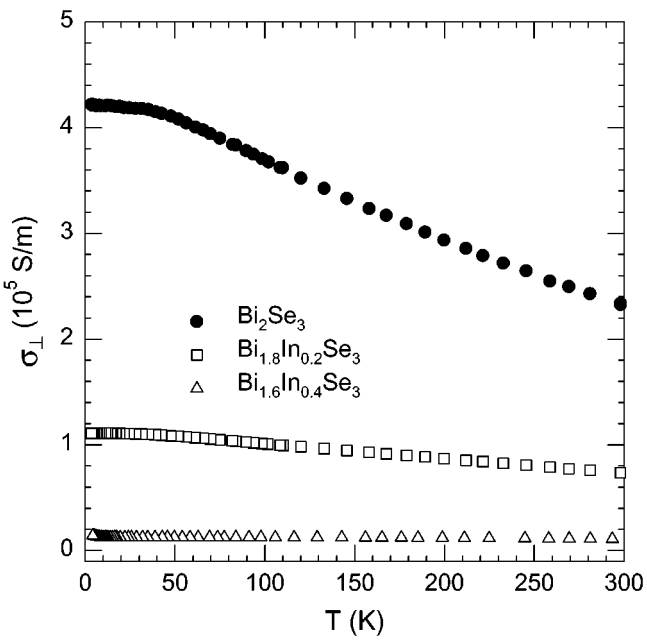

FIG. 1. Temperature dependence of electrical conductivity of $Bi_{2-x}In_xSe_3$ crystals.

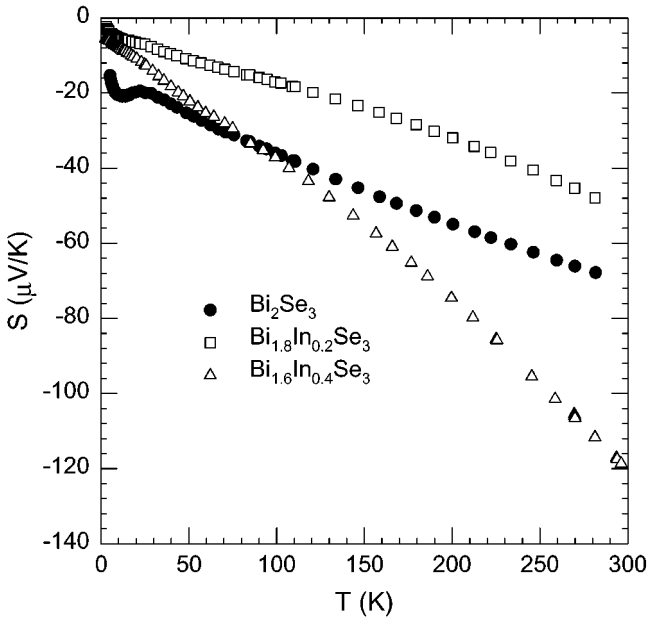

FIG. 2. Temperature dependence of Seebeck coefficient of $Bi_{2-x}In_xSe_3$ crystals.

(b) although scattering on the acoustic branch of lattice vibrations prevails at room temperature in Bi_2Se_3, a contribution due to scattering by ionized impurities has to be taken into account,

(c) the calculated value of the effective mass determined at 300 K is taken as constant in the temperature range covered (this is our simplifying assumption).

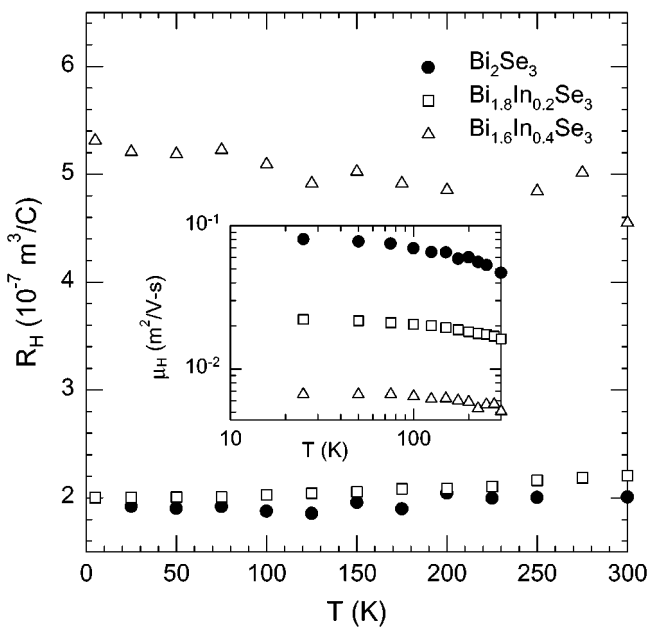

FIG. 3. Temperature dependence of Hall constant and Hall mobility (inset) of $Bi_{2-x}In_xSe_3$ crystals.

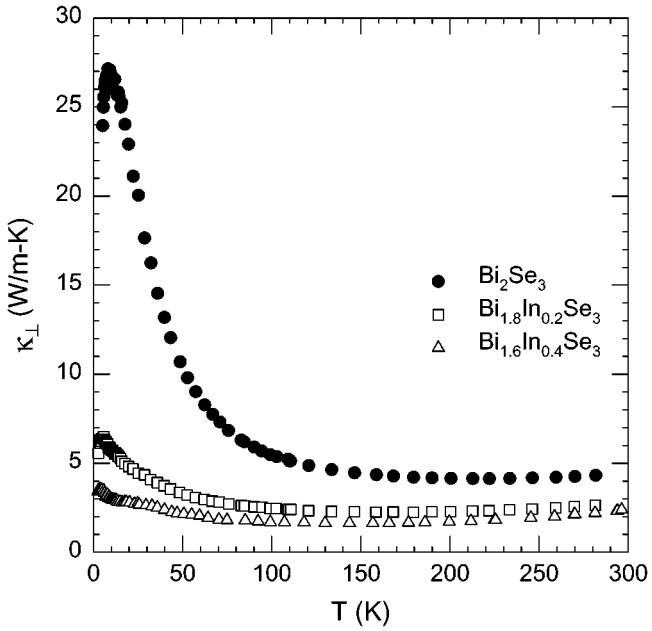

FIG. 4. Temperature dependence of total thermal conductivity of $Bi_{2-x}In_xSe_3$ crystals.

In the presence of both acoustic phonon and ionized impurity scattering, one can express the overall mixed scattering time (11) as

$$\frac{1}{\tau} = \frac{1}{\tau_{\mathrm{ph}}} + \frac{1}{\tau_{\mathrm{ion}}}. \qquad [1]$$

Because $\tau_{\mathrm{ph}} = \tau_{0\mathrm{L}}\varepsilon^{-1/2}$ and $\tau_{\mathrm{ion}} = \tau_{0\mathrm{i}}\varepsilon^{3/2}$, where ε is reduced energy of electrons, the relaxation time can be written in terms of the carrier energy as

$$\tau(\varepsilon) = \frac{\tau_{0\mathrm{L}}\varepsilon^{3/2}}{\varepsilon^2 + a^2}, \qquad [2]$$

where $a^2 = \tau_{0\mathrm{L}}/\tau_{0\mathrm{i}}$. Integration of the general expression of the electrical conductivity σ, using $\tau(\varepsilon)$ from Eq. [2], leads, according to the Fistul formalism (11), to the following expression for the electrical conductivity in the direction perpendicular to the c-axis:

$$\sigma_{\perp} = \frac{8\pi e^2 (2m_{\mathrm{d}}kT)^{3/2}}{3m_{\perp}h^3}\,\tau_{0\mathrm{L}}\Phi_3(\eta, a_{\perp}). \qquad [3]$$

Here, $m_{\perp}$ is the effective mass of electrons in the direction perpendicular to the c-axis, m_{d} is the density of states effective mass, k is the Boltzmann constant, $\eta = \varepsilon_{\mathrm{F}}/kT$ is the reduced Fermi energy, and $\Phi_3(\eta, a)$ is a two-parameter integral which can generally be expressed as

$$\Phi_{\mathrm{n}} = \int_0^{\infty} \frac{\varepsilon^{\mathrm{n}} e^{\varepsilon - \eta}}{(\varepsilon^2 + a^2)(1 + e^{\varepsilon - \eta})^2}\, d\varepsilon. \qquad [4]$$

The Seebeck coefficient is then

$$S_{\nabla T \perp c} = -\frac{k}{e}\left[\frac{\Phi_4(\eta, a_\perp)}{\Phi_3(\eta, a_\perp)} - \eta\right] \qquad [5]$$

and the Hall coefficient is given by

$$R_H(B \| c) = \frac{A_\perp \gamma}{ne} = \frac{3}{2}\frac{F_{1/2}(\eta)\Phi_{9/2}(\eta, a_\perp)}{[\Phi_3(\eta, a_\perp]^2}\frac{1}{ne}, \qquad [6]$$

where γ is the structural factor ($\gamma \approx 1$) and $A_\perp$ is the Hall factor. Integral $\Phi_{9/2}(\eta, a)$ in Eq. [6] differs from the general expression for the two-parameter integrals (see Eq. [4]) only in the denominator term: $(\varepsilon^2 + a^2)^2$ instead of $(\varepsilon^2 + a^2)$.

The concentration of free carriers is given by

$$n = 4\pi\left(\frac{2m_d kT}{h^2}\right)^{3/2} F_{1/2}(\eta). \qquad [7]$$

The density of states effective mass at the conduction band edge is, in this case, given as

$$m_d = (m_\perp^2 m_\parallel)^{1/3}. \qquad [8]$$

Measurements of the reflectance in the plasma resonance frequency (ω_p) region were used to determine effective masses $m_\perp$ and m_d. The $\omega_p(E \perp c)$ for the incident radiation perpendicular to the c-axis can be expressed as

$$\omega_p^2(E \perp c) = \frac{ne^2}{\varepsilon_0 \varepsilon_\infty m_0 m_\perp}, \qquad [9]$$

where ε_0 is the permittivity of free space. If measurements of the reflectance in both perpendicular and parallel directions to the c-axis are available, one can simply derive the expression

$$\frac{\omega_p^2(E \perp c)}{\omega_p^2(E \| c)} = \frac{\varepsilon_{\infty\parallel} m_\parallel}{\varepsilon_{\infty\perp} m_\perp}, \qquad [10]$$

where $\varepsilon_{\infty\perp}$ and $\varepsilon_{\infty\parallel}$ are high-frequency permittivities in perpendicular and parallel directions with respect to the c-axis. This approach was used in (12) for Bi_2Se_3 and we obtained averaged values of $m_\parallel/m_\perp = 3.87$ in this work.

Supposing that the value of the Hall factor is very close to unity due to a rather high concentration of electrons, we were able, from Eqs. [6] to [9], to obtain the following values for Bi_2Se_3 at 300 K:

$$n = 2.88 \times 10^{25}\ \mathrm{m}^{-3},\ \eta = 5.53,\ m_\perp = 0.150\, m_0,$$

and

$$m_d = 0.236\, m_0.$$

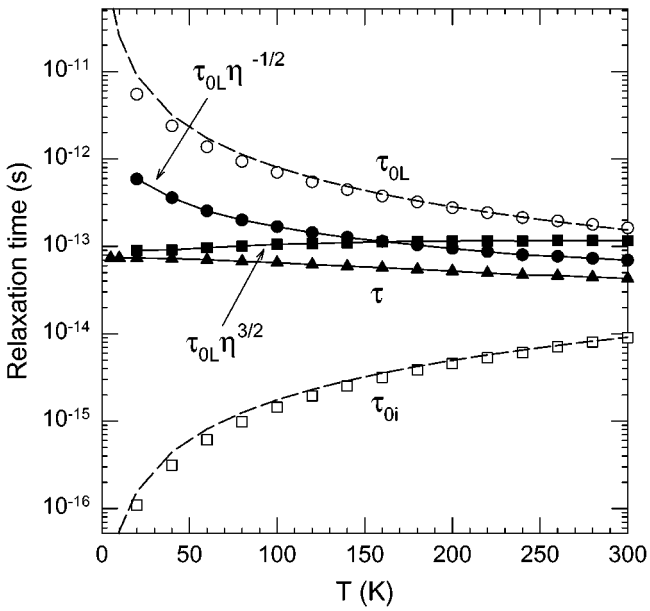

FIG. 5. Calculated relaxation times τ_{0L} and τ_{0i} (empty symbols) of Bi_2Se_3 crystal. Dashed lines represent theoretical temperature dependencies $\tau_{0L} \sim T^{-3/2}$ and $\tau_{0i} \sim T^{3/2}$, respectively. Full symbols represents products of $\tau_{0L}\eta^{-1/2}$ and $\tau_{0i}\eta^{3/2}$ and total relaxation time, where η is the reduced Fermi energy. The relaxation time τ was calculated from the experimental values of the conductivity and the carrier concentration using the Drude approach via Eqs. [1]–[3].

From the equations for the electrical conductivity [3] and Seebeck coefficient [5] one is then able to determine temperature dependencies of the relaxation times τ_{0L} and τ_{0i}. In Eq. [2], ε corresponds to the mean electron energy. In the case where the carriers are distributed in bands according to Fermi–Dirac statistics the energy is equal to the reduced Fermi level η (11). Temperature dependencies of the individual relaxation times and their products $\tau_{0L}\eta^{-1/2}$ and $\tau_{0i}\eta^{3/2}$ are presented in Fig. 5. It can be seen from the figure that $\tau_{0L} \sim T^{-3/2}$, while $\tau_{0i} \sim T^{3/2}$. One can then say that the slight temperature dependence of the experimentally determined relaxation time $\tau(\equiv \sigma_\perp m_\perp^*/e^2 n)$ could be accounted for with mixed free carrier scattering on acoustic phonons and on ionized impurities. We note that at $T < 30$ K disagreement with this model was observed. In our opinion, very weak temperature dependence of the mobility and relaxation time at low temperatures indicates another possible interpretation, i.e., existence of neutral impurity scattering as an important scattering mechanism. Therefore, we tried to interpret the temperature dependence of the relaxation time using a mixed scattering mechanism on acoustic phonons and on neutral impurities. Unfortunately, this combination also led to less than satisfying results.

From determined values of the Fermi level η and a-parameter, the Lorenz number L and electronic

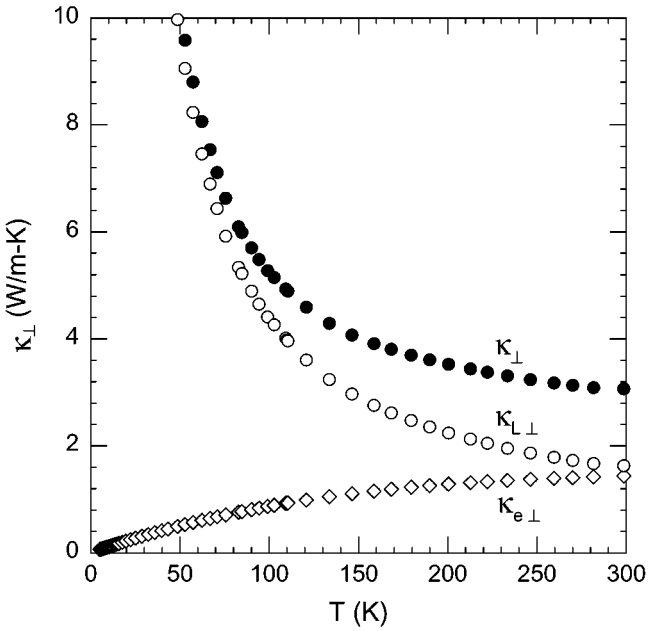

FIG. 6. Temperature dependence of thermal conductivity and of its electronic and lattice components measured on a single crystal of Bi_2Se_3 in the direction perpendicular to the trigonal axis (*c*-axis).

component of the thermal conductivity $\kappa_{e\perp}$ were calculated using the formula.

$$\frac{\kappa_{e\perp}}{\sigma_\perp T} = L = \frac{k^2}{e^2}\frac{\Phi_3\Phi_5(\eta, a_\perp) - \Phi_4^2(\eta, a_\perp)}{\Phi_3^2(\eta, a_\perp)}. \qquad [11]$$

Values of the Lorenz number calculated using Eq. [11] are up to 25% smaller than the Sommerfeld value of $2.44 \times 10^{-8}\ V^2/K^2$ and reflect the partial inelasticity of the carrier scattering. The lattice thermal conductivity, $\kappa_{L\perp}$, is then obtained by subtracting the electronic component from the total thermal conductivity, $\kappa_\perp$. All three components ($\kappa_\perp, \kappa_{e\perp}, \kappa_{L\perp}$) are displayed in Fig. 6. It is evident that the electronic component for undoped Bi_2Se_3 at 300 K ($\kappa_{e\perp} = 1.44\ W\,m^{-1}\,K^{-1}$) is comparable to the lattice contribution ($\kappa_{L\perp} = 1.63\ W\,m^{-1}\,K^{-1}$).

$Bi_{2-x}In_xSe_3$ Single Crystals

As the band structure of these crystals has not been studied yet, we used a simplified model to describe the transport properties of $Bi_{2-x}In_xSe_3$. This model is characterized by the following three features:

(a) Just as in the case of pure Bi_2Se_3, the conduction band of $Bi_{2-x}In_xSe_3$ crystals can also be described in terms of a single-valley one-conduction-band model,

(b) the density of states effective mass determined at 300 K does not change significantly in the studied temperature range,

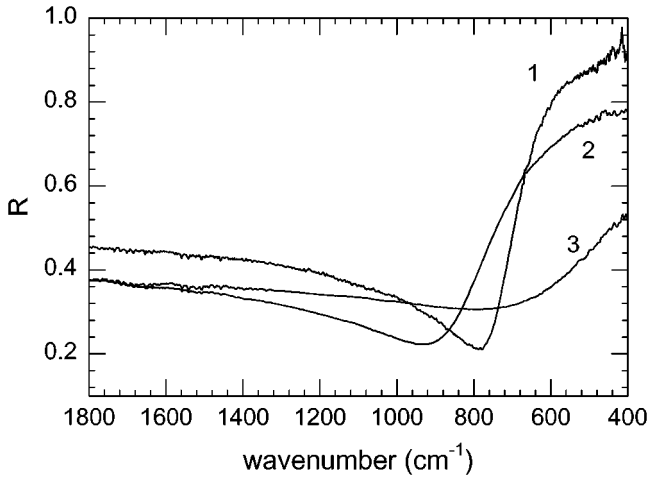

FIG. 7. Reflectance spectra of the $Bi_{2-x}In_xSe_3$ single crystals at room temperature: (1) Bi_2Se_3; (2) $Bi_{1.8}In_{0.2}Se_3$; (3) $Bi_{1.6}In_{0.4}Se_3$.

(c) the contribution of carrier scattering by ionized impurities at 300 K is neglected, but at low temperatures should be considered.

Assumption (c) is supported by the reflectance spectrum analysis of the studied crystals. In the plasma resonance frequency region, the reflectance spectra were fitted (see Fig. 7) using equations for the real and imaginary parts of the complex dielectric function (6). The obtained values of the high-frequency permittivity $\varepsilon_{\infty\perp}$, the plasma resonance frequency ω_p, the ratio $n/m_\perp$, and the optical relaxation time $\tau_{\perp opt}$ are given in Table 1.

Frequency dependence of the imaginary part of the dielectric function, ε_2, allows one to evaluate the dominant type of scattering mechanism of charge carriers. In the frequency region where the scattering is due to free carriers and interband transitions, the imaginary part of the dielectric function is given by the expression $\varepsilon_2 = \varepsilon_2^{FC} + \varepsilon_2^{IB}$, where ε_2^{FC} is the contribution of free current carriers and ε_2^{IB} is the contribution of interband transitions. According to (13), the frequency dependence of ε_2^{FC} is given by the relation $\varepsilon_2^{FC} \sim \bar{v}^{-\beta}$ (where β is the exponent characteristic of the scattering mechanism). This dependence holds for $hvc \gg 2kT$.

As discussed in (13), the value of the exponent $\beta = 2.5$ corresponds to the scattering of free current carriers on

TABLE 1
Optical Parameters of $Bi_{2-x}In_xSe_3$ Single Crystals

	$\varepsilon_{\infty\perp}$ [—]	ω_p ($E\perp c$) [$10^{14}\,s^{-1}$]	$n/m_\perp$ [$10^{26}\,m^{-3}$]	$\tau_{\perp opt}$ [$10^{-14}\,s$]
Bi_2Se_3	29.8	1.42	1.89	4.50
$Bi_{1.8}In_{0.2}Se_3$	22.0	1.60	1.75	2.30
$Bi_{1.6}In_{0.4}Se_3$	18.3	1.20	0.83	1.05

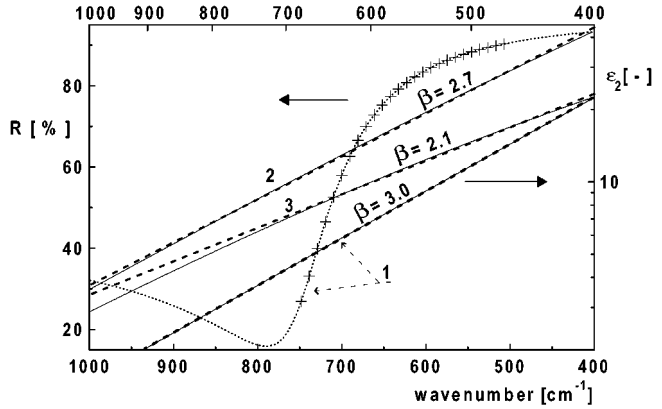

FIG. 8. Logarithmic dependence ε_2 vs $\bar{\nu}$ [cm^{-1}] (solid lines) with linear fits (dashed lines) in the resonance plasma frequency region. Reflectance spectrum of Bi_2Se_3 (dotted line) with marked region (crosses) where contribution of the free carriers to ε_2 prevails and from which β values were determined.

acoustic phonons, and $\beta = 4.5$ corresponds to the scattering by ionized impurities. According to our results presented in Fig. 8, the exponent $\beta = 3.0$ for undoped Bi_2Se_3, while for $Bi_{2-x}In_xSe_3$ single crystals β was found to be near 2.5. We can therefore state that for $Bi_{2-x}In_xSe_3$ crystals the charge carriers are predominantly scattered by acoustic phonons.

Thus, from the reflectance data and a simplified equation for the Hall coefficient ($R_H = 1/ne$), effective masses $m_\perp$ of both $Bi_{2-x}In_xSe_3$ crystals ($x = 0.2$ and $x = 0.4$) at 300 K were determined. The resulting values are: $0.155m_0$ for $Bi_{1.8}In_{0.2}Se_3$, and $0.159m_0$ for $Bi_{1.6}In_{0.2}Se_3$. These values are slightly higher than the $m_\perp$ value for pure Bi_2Se_3 ($0.15m_0$). Values of η and m_d were determined from Eqs. [5] and [7] assuming purely acoustic scattering at 300 K (i.e., $a_\perp = 0$). At lower temperatures the presence of ionized impurity scattering was considered and Eqs. [1]–[3] were used to obtain the temperature dependencies of the relaxation times τ_{0L} and τ_{0i} for both In-substituted crystals (see Figs. 9 and 10). The calculated values of τ_{0L} and τ_{0i} are close to the theoretical temperature dependencies of the respective relaxation times.

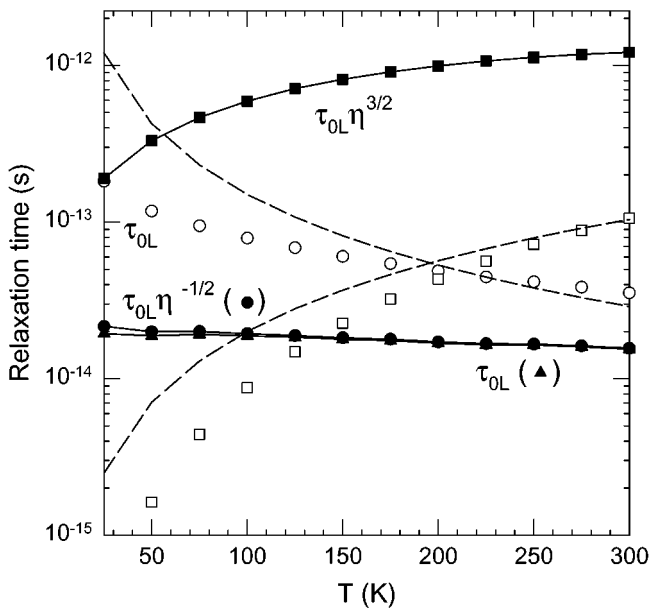

FIG. 9. Calculated relaxation times τ_{0L} and τ_{0i} (empty symbols) of $Bi_{1.8}In_{0.2}Se_3$ crystal. Dashed lines represent theoretical temperature dependencies $\tau_{0L} \sim T^{-3/2}$ and $\tau_{0i} \sim T^{3/2}$, respectively. Full symbols represent products of $\tau_{0L}\eta^{-1/2}$ and $\tau_{0i}\eta^{3/2}$ and total relaxation time, where η is the reduced Fermi energy. The relaxation time τ was calculated from the experimental values of the conductivity and the carrier concentration using the Drude approach via Eqs. [1]–[3].

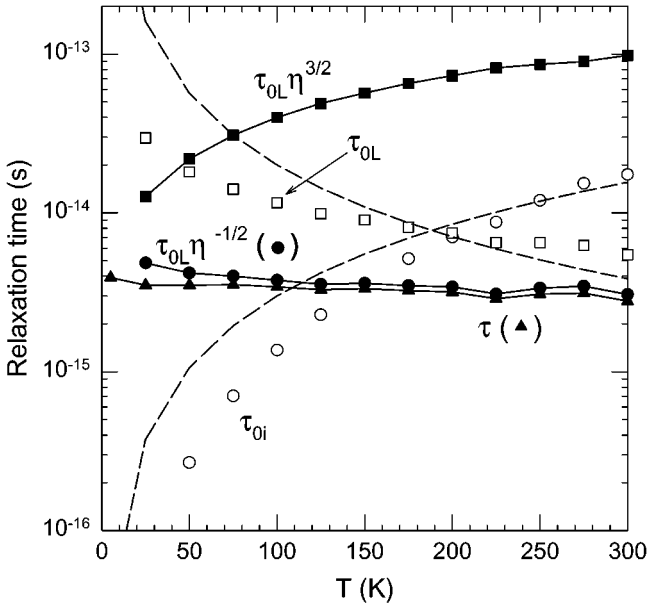

FIG. 10. Calculated relaxation times τ_{0L} and τ_{0i} (empty symbols) of $Bi_{1.6}In_{0.4}Se_3$ crystal. Dashed lines represent theoretical temperature dependencies $\tau_{0L} \sim T^{-3/2}$ and $\tau_{0i} \sim T^{3/2}$, respectively. Full symbols represent products of $\tau_{0L}\eta^{-1/2}$ and $\tau_{0i}\eta^{3/2}$ and total relaxation time, where η is the reduced Fermi energy. The relaxation time τ was calculated from the experimental values of the conductivity and the carrier concentration using the Drude approach via Eqs. [1]–[3].

The electronic thermal conductivity was calculated with the aid of Eq. [11]. The temperature dependence of $\kappa_\perp$, $\kappa_{e\perp}$, and $\kappa_{L\perp}$ of these mixed crystals is presented in Fig. 11 and their room temperature values are given in Table 2. It is evident that the overall thermal conductivity as well as its electronic and lattice components are significantly smaller upon incorporation of In into the crystal structure, and this trend is magnified as the content of In is increased. Thus, referring to the two samples containing indium, the lower carrier density in $Bi_{1.6}In_{0.4}Se_3$ in relation to $Bi_{1.8}In_{0.2}Se_3$ leads to its reduced electronic thermal conductivity component, while its higher In content has a detrimental effect on the lattice thermal conductivity. The room temperature values of the relevant transport parameters of all the crystals

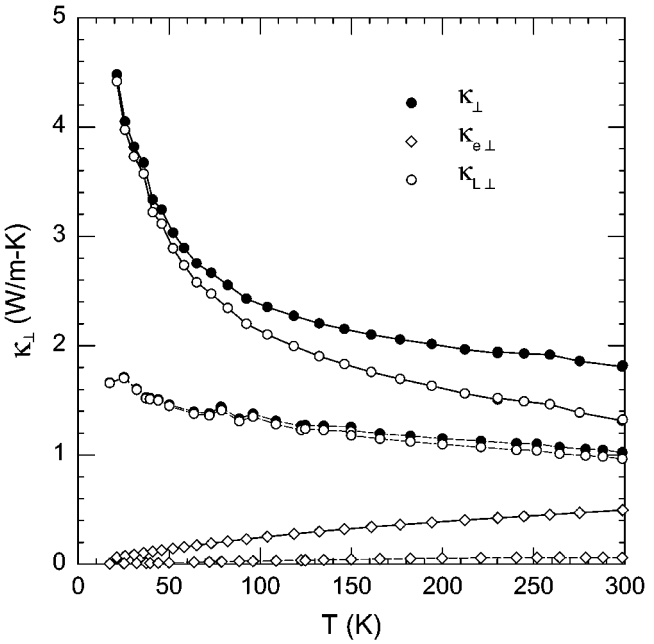

FIG. 11. Temperature dependence of thermal conductivity and of its electronic and lattice components measured on single crystals of $Bi_{1.8}In_{0.2}Se_3$ (solid lines) and $Bi_{1.6}In_{0.4}Se_3$ (dashed lines). All measurements are perpendicular to the trigonal axis (*c*-axis).

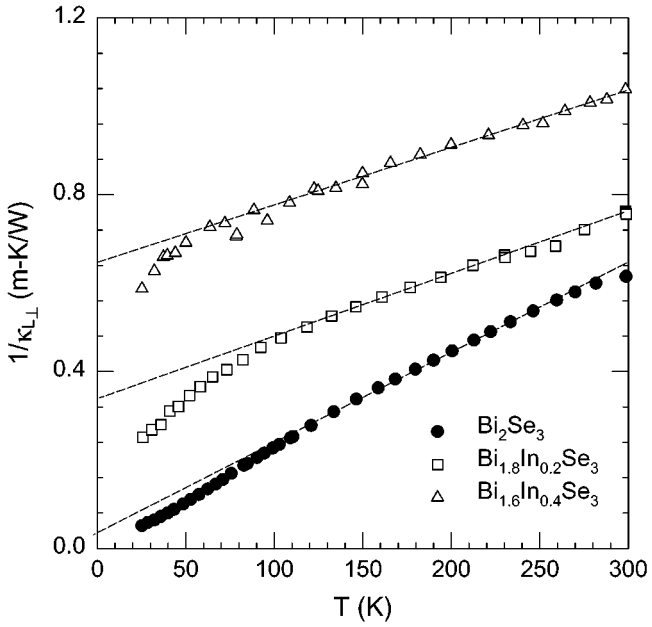

FIG. 12. Temperature dependence of the lattice thermal resistivity of the $Bi_{2-x}In_xSe_3$ single crystals.

are summarized in Table 2. The reduced values of $\kappa_{L\perp}$ following the incorporation of In atoms into the Bi_2Se_3 crystal lattice indicate that phonons scatter strongly on In_{Bi}^{x} substitutional defects.

The temperature dependence of the thermal resistance $W_L(\equiv 1/\kappa_L)$ of all crystals is linear in the range 100–300 K (see Fig. 12) and could be expressed as

$$W_L = AT + B = W_L^0 + \Delta W, \qquad [12]$$

where W_L^0 is the lattice thermal resistance of an undoped crystal and ΔW represents a contribution to the resistance arising from the presence of impurities and lattice defects. In accord with the experiments carried out on semiconducting crystals of similar type, the $W_L(T)$ dependence of the undoped Bi_2Se_3 crystal has a small, but nonzero *y*-intercept, specifically $\Delta W = 0.03\ W\,m^{-1}\,K^{-1}$. This indicates that Bi_2Se_3 prepared under these conditions contains a certain concentration of natural point defects: $V_{Se}^{\cdot\cdot}$ (vacancy on a Se site with two localized positive charges) and $Bi_{Se}^{\prime}$ (Bi on a Se site carrying one localized electron). For In-doped crystals, the ΔW term increases significantly with the increasing In content. Accordingly, $\Delta W(Bi_{1.8}In_{0.2}Se_3) = 0.33\ W\,m^{-1}\,K^{-1}$ and $\Delta W(Bi_{1.6}In_{0.4}Se_3) = 0.64\ W\,m^{-1}\,K^{-1}$.

The influence of In on the thermal transport is also evident from Fig. 13, where logarithmic plot of temperature dependence of lattice thermal conductivity is presented. One can see that for an undoped Bi_2Se_3 crystal $\kappa_{L\perp} \sim T^{-1}$. Upon adding In, the temperature dependence of $\kappa_{L\perp}$ becomes considerably weaker than $1/T$. The T^{-1} dependence observed for undoped Bi_2Se_3 indicates that phonon scattering at $T > \Theta_D$ (Θ_D being the Debye temperature) in this structure consists of normal three-phonon and Umklapp processes (14). In In-doped Bi_2Se_3 crystals, there is a clear indication of the presence and influence of point defect

TABLE 2
Physical Parameters of $Bi_{2-x}In_xSe_3$ Crystals at 300 K

	$\kappa_\perp$ [$Wm^{-1}K^{-1}$]	n [$10^{25}m^{-3}$]	E_F [eV]	$a_\perp^2$ [—]	$R_H\sigma_\perp$ [$m^2V^{-1}s^{-1}$]	$\kappa_{\perp e}$ [$Wm^{-1}K^{-1}$]	$\kappa_{\perp L}$ [$Wm^{-1}K^{-1}$]	ZT [—]
Bi_2Se_3	3.07	2.8	0.140	15	0.0467	1.44	1.63	0.11
$Bi_{1.8}In_{0.2}Se_3$	1.82	2.8	0.143	≈ 0	0.0162	0.49	1.33	0.03
$Bi_{1.6}In_{0.4}Se_3$	1.02	1.4	0.069	≈ 0	0.0051	0.06	0.96	0.05

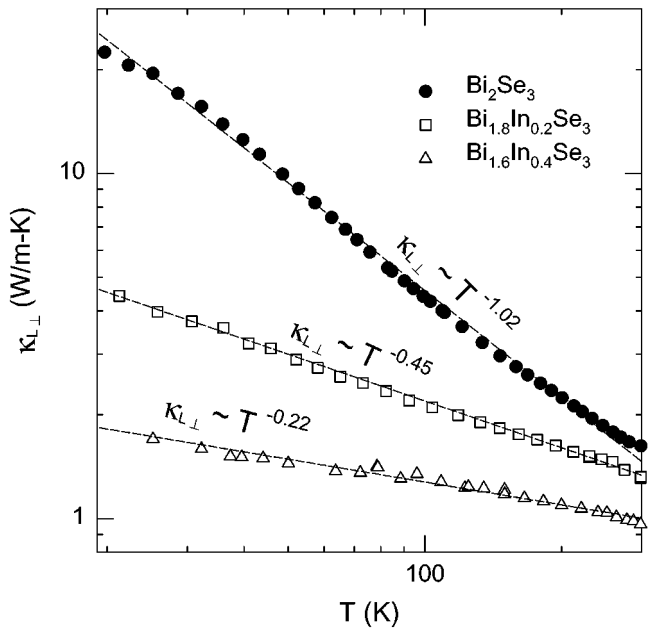

FIG. 13. Logarithmic plot of temperature dependence of lattice thermal conductivity of the $Bi_{2-x}In_xSe_3$ single crystals.

scattering in addition to the normal and Umklapp processes.

CONCLUSIONS

The experimental results lead to the following conclusions:

(1) The incorporation of In atoms into the Bi_2Se_3 crystal lattice causes a rapid decrease in the mobility of free charge carriers and, consequently, a significant suppression of the electronic thermal conductivity. This result is in accord with a considerable decrease observed in the optical relaxation time with increasing In content.

(2) It follows from the analysis of the carrier mobility that its weak temperature dependence can be explained by using a model of mixed scattering whereby the charge carriers scatter on acoustic phonons and ionized impurities. In the case of Bi_2Se_3, ionized impurity scattering extends to room temperature. The incorporation of In atoms into Bi_2Se_3 tends to suppress the contribution of this mechanism.

(3) The presence of In atoms in the Bi sublattice—the formation of uncharged substitution defects $In^{\times}_{Bi}$ of indium atoms on bismuth sites—influences the concentration of native defects in the crystals. The increasing density of $In^{\times}_{Bi}$ defects results in an increase in the bond polarity and in the crystal ionicity. The consequence is a suppression of the overstoichiometry of Bi atoms in the crystal lattice. This leads to a decrease in the density of Se vacancies ($V^{\cdot\cdot}_{Se}$) and a reduction in the free carrier concentration. This effect was described in detail in (7).

(4) The thermal conductivity decreases upon incorporation of In into the crystal lattice of Bi_2Se_3 because the electronic as well as the lattice thermal conductivity are suppressed by the presence of In. As for the lattice thermal conductivity, it is evident that while in undoped Bi_2Se_3 the phonon scattering mechanism is dominated by normal three-phonon and Umklapp processes only, in In-doped crystals phonon scattering by point defects plays an important role.

(5) From the experimental data it follows that incorporation of In into the crystal lattice of Bi_2Se_3 leads to a significant degradation in the thermoelectric figure of merit. For this reason, alloys of composition $Bi_{2-x}In_xSe_3$ appear unlikely to be prospective thermoelectric materials.

ACKNOWLEDGMENTS

We gratefully acknowledge research support provided by NATO Grant HTECH CRG 873186 and by DARPA Contract N00014-98-3-0011.

REFERENCES

1. H. J. Goldsmid, "Thermoelectric Refrigeration." Pion Ltd., London, 1986.
2. D. P. Belotskii and N. V. Demyanchuk, *Izv. Akad. Nauk SSSR Neorg. Mater.* **5,** 1518–1521 (1969).
3. H. G. Bouanani, D. Eddike, B. Liautard, and G. Brun, *Mater. Res. Bull.* **31,** 177–187 (1996).
4. D. P. Belotskii, P. F. Babyuk, N. V. Demyanchuk, N. P. Novalkovskii, and R. F. Boichuk, *in* "Nizkotemperaturnye Termoelektricheskie Materialy" (D. V. Gitsu, Ed.), pp. 29–35. Red. -Izd. Otd. Akad. Nauk. Mold. SSR, Kishinev, 1970.
5. P. Lošťák, L. Beneš, S. Civiš, and H. Süssmann, *J. Mater. Sci.* **25,** 277–282 (1990).
6. P. Lošťák, R. Novotný, E. Urbanová, and J. Horák, *Phys. Status Solidi A* **113,** 615–622 (1989).
7. J. Horák, Z. Starý, P. Lošťák, and J. Pancíř, *J. Phys. Chem. Solids* **51,** 1353–1360 (1990).
8. K. Yokota and S. Katayama, *Jpn. J. Appl. Phys.* **12,** 1205 (1973).
9. H. Köhler and A. Fabricius, *Phys. Status Solidi B* **71,** 487–496 (1975).
10. V. A. Kulbachinskii, N. Miura, H. Nakagawa, H. Arimoto, T. Ikaida, P. Lošťák, and Č. Drašar, *Phys. Rev. B* **59,** 15,733–15,739 (1999).
11. V. I. Fistul, "Silno Legirovanye Poluprovodniki." Izd. Nauka, Moscow, 1969.
12. M. Stordeur, K. K. Ketavong, A. Priemuth, H. Sobotta, and V. Riede, *Phys. Status Solidi B* **169,** 505–514 (1992).
13. K. Seeger, "Semiconductor Physics." Springer-Verlag, Vienna, 1973.
14. J. Callaway, *Phys. Rev.* **113,** 1046 (1959).